Green-Ampt infiltration model for sloping surfaces

Li Chen[1] and Michael H. Young[1]

Received 27 July 2005; revised 31 March 2006; accepted 19 April 2006; published 27 July 2006.

[1] This work quantifies and explains the direct physical effects of slope angle on infiltration and runoff generation by extending the Green-Ampt equation onto sloping surfaces. A new extended solution using identical precipitation hydrographs was compared to the original formulation and then used to calculate the infiltration and runoff generation for different slope angles but for identical horizontal projection lengths. Homogeneous and isotropic soil is assumed, and two different boundary conditions for vertical rainfall are studied: ponded infiltration and infiltration under steady rainfall. Infiltration under unsteady rainfall was found to be similar to cases with steady rainfall. Both theoretical and numerical results show that infiltration increases with increasing slope angle. For cases with ponded infiltration the slope effect was generally not significant for mild to moderate slopes, but the slope effect became more important for low-intensity and short-duration rainfall events, especially as it delayed the time for ponding. It was also found that the cumulative vertical infiltration depth (I_{hp}) at ponding (or the initial loss) increases with increasing slope angle. The model was compared to Richards' equation on horizontal and sloping surfaces and found to perform well. The model's applicability for nonuniform slopes was discussed, and it was found that the model is generally applicable for isotropic and mildly anisotropic soils except for some small-scale topographic elements. Finally, the occurrence of nonvertical rainfall could increase runoff with increasing slope angle when rainfall deflects a large angle to upslope.

Citation: Chen, L., and M. H. Young (2006), Green-Ampt infiltration model for sloping surfaces, *Water Resour. Res.*, *42*, W07420, doi:10.1029/2005WR004468.

1. Introduction

[2] Hillslope hydrology has received significant attention during the past several decades [e.g., *Kirkby*, 1978; *Philip*, 1991; *Torres et al.*, 1998]. The degree of land sloping has been included as an important factor in numerous studies because it is closely related to many environmental processes, such as surface and subsurface water movement, soil erosion, debris flow, and landslides. For example, the widely used soil erosion prediction model universal soil loss equation (USLE) [*Wischmeier and Smith*, 1978] directly includes a slope length-slope gradient factor in the model equation. The effect of slope on rainfall-runoff generation processes is a fundamental aspect of the use of this approach. Indoor experiments and field observations on runoff generation have been used to these effects; however, it still remains as a controversial problem. For example, *Poesen* [1984] and *Govers* [1991] both observed a decrease in runoff with increasing slope; but other researchers [e.g., *De Ploey et al.*, 1976; *Djorovic*, 1980; *Sharma et al.*, 1983, 1986; *Fox et al.*, 1997; *Chaplot and Le Bissonnais*, 2000] observed an increase in runoff with increasing slope angle. Still others [*Lal*, 1976; *Mah et al.*, 1992; *Grosh and Jarrett*, 1994] found no significant effect of slope angle on runoff. Different researchers attribute the different trends to various factors. *Poesen* [1984] attributed the decreasing runoff to either a thinning of the soil crust or to increasing infiltration by increasing rilling erosion. *Govers* [1991] found that the negative slope effect was also related to differential soil cracking. *De Ploey et al.* [1976], *Sharma et al.* [1983], *Djorovic* [1980] and *Fox et al.* [1997] attributed the negative slope effect to a decrease in depressional surface storage and ponding depth. In each case listed above, site-specific conditions likely affected their observations, making generalizations difficult to verify. Crusting, rilling and small topographic structures may play important roles in rainfall-runoff processes; however, they are indirect and may not necessarily appear on sloping surfaces, though they may significantly affect processes once they occur.

[3] This study focuses on the direct impact that slope steepness has on infiltration and runoff generation processes, and addresses questions of whether and how slope angle affects rainfall-runoff processes on landscapes with slopes, versus landscapes without slopes. The question becomes important because a commonly used approach for simulating infiltration is the Green-Ampt (GA) model, which has not been modified to account for sloping landscapes. The GA model treats all land surfaces as horizontal planes, even though surfaces may be physically sloped. To account for this deficiency, this study extends the GA model to account for sloping surfaces, while assuming homogeneous and isotropic soil properties, as is done in most rainfall-runoff models (e.g., HEC-1 [*U.S. Army Corps of Engineers*, 1998]). The analysis of infiltration between horizontal plane and sloping surface assumes the same horizontal projection

[1]Division of Hydrologic Sciences, Desert Research Institute, Las Vegas, Nevada, USA.

0043-1397/06/2005WR004468$09.00

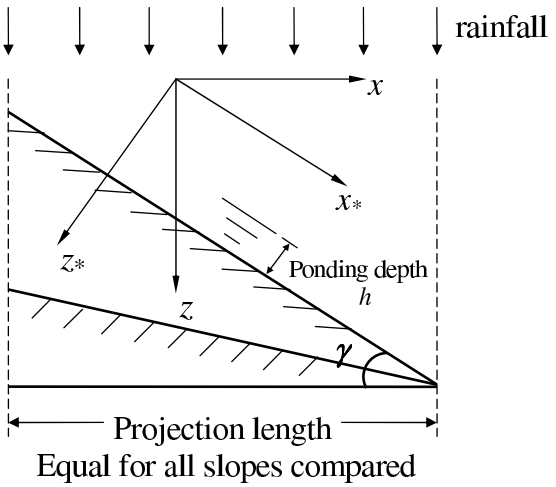

Figure 1. Definition of study system.

length rather than the same slope length to ensure the rainfall amount received at different surfaces is the same (Figure 1). This approach is necessary only for runoff volume analysis. It does not affect the infiltration comparison.

[4] The Green-Ampt model [*Green and Ampt*, 1911] is a simplified representation of the infiltration process. It assumes a homogeneous soil profile and a uniform distribution of initial soil water content. The model assumes that a wetting front is present in the soil profile, and that the front separates the profile into an upper saturated zone and a lower unsaturated zone, where the water content is kept at the initial soil value. Lateral movement of soil water content is neglected, even in cases where the land surface is no longer perpendicular to the gravity vector. After the original model was presented by *Green and Ampt* [1911], it was modified by scientists. For example, *Mein and Larson* [1973] extended the model from ponded infiltration to a constant intensity rainfall input condition, and *Chu* [1978] applied this model to an unsteady rainfall distribution. Neither of these modifications dealt with the cases of sloping landscapes. In the present paper (and as has been done in the past) the GA model is treated as an approximation to Richards' equation. Therefore Richards' equation for sloping surfaces is described, and then followed with the derivation of the GA model for a number of surface boundary conditions.

2. Richards' Equation on Sloping Surfaces

[5] The general form of Richards' equation reads

$$\frac{\partial \theta}{\partial t} = \nabla \cdot (D \nabla \theta) - \frac{dK}{d\theta}\frac{\partial \theta}{\partial z} \tag{1}$$

where θ is water content, D is soil water diffusivity ($m^2\ s^{-1}$), K is hydraulic conductivity ($m\ s^{-1}$), z is vertical spatial coordinate (m), and t is time (s).

[6] For one-dimensional vertical infiltration on a horizontal plane, the equation reads

$$\frac{\partial \theta}{\partial t} = \frac{\partial}{\partial z}\left(D\frac{\partial \theta}{\partial z}\right) - \frac{dK}{d\theta}\frac{\partial \theta}{\partial z} \tag{2}$$

The coordinates x_* and z_* are defined in the downslope and normal directions (Figure 2), so that Equation (2) can be rewritten as

$$\frac{\partial \theta}{\partial t} = \nabla \cdot (D \nabla \theta) - \frac{dK}{d\theta}\left(\frac{\partial \theta}{\partial x_*}\sin\gamma + \frac{\partial \theta}{\partial z_*}\cos\gamma\right) \tag{3}$$

where γ is the slope angle.

[7] From *Philip* [1991], the solution to equation (3) on a planar slope is independent of x_* except for a small region from the crest or the point of the slope change. Therefore equation (3) can be simplified to

$$\frac{\partial \theta}{\partial t} = \frac{\partial}{\partial z_*}\left(D\frac{\partial \theta}{\partial z_*}\right) - \frac{dK}{d\theta}\frac{\partial \theta}{\partial z_*}\cos\gamma \tag{4}$$

This indicates that except for the difference of coordinate definition, the only change needed to use equation (4) on sloping surfaces is to replace K with $K\cos\gamma$. The dynamic meaning of this modification is that on sloping surfaces, only gravity normal to the surface direction is changed by $\cos\gamma$ (i.e., capillary forces are unchanged). Conversely, the downslope component of gravity does cause flow, but it does not change the water content profile along the normal direction on a planar slope because the flow field is independent of x_*. Therefore, as an approximate solution, the GA model can be redefined with this same modification.

3. Green-Ampt Model on Sloping Surfaces

3.1. Ponded Infiltration

[8] On the basis of Darcy's law, the GA model for the sloping surface under ponding condition can be expressed in the following form:

$$i = i_c = K_e\frac{z_{*f}\cos\gamma + s_f + H}{z_{*f}} \tag{5}$$

where i_c is infiltrability equal to the infiltration rate i for ponded infiltration (m), K_e is effective saturated hydraulic conductivity, z_{*f} is wetting front depth in the direction normal to the land surface, s_f is the wetting front matric potential, H is the ponding water head-on the ground surface, and $z_{*f}\cos\gamma$ represents gravity head at the wetting front. Physically, every variable is assumed to remain constant along the downslope direction.

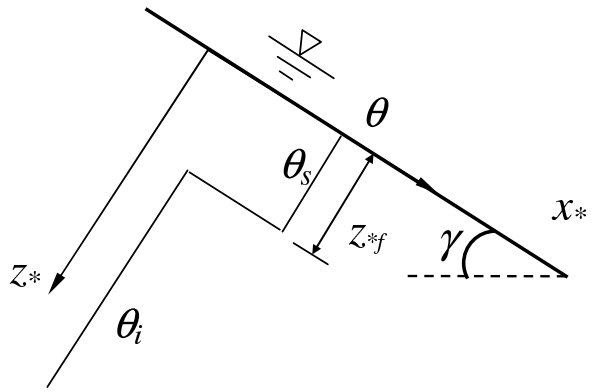

Figure 2. Sketch of the step function of water content profile for sloping land surface.

[9] Note that the ponding water head-on sloping lands, H, is not the ponding depth h normal to the land surface (Figure 1); here, H equals $h \cos \gamma$. Usually, the ponding depth on a sloping surface is small compared to the wetting front matric potential, s_f. Therefore a small ponding water head was assumed for the theoretical analysis in this study and treated as a revision to s_f. The cumulative infiltration depth in the normal direction, I, can be expressed as

$$I = (\theta_s - \theta_i) z_{*f} \tag{6}$$

Taking the derivative of I with respect to time and substituting into equation (5) yields

$$\frac{dz_{*f}}{dt} = \frac{K_e}{(\theta_s - \theta_i)} \frac{z_{*f} \cos \gamma + s_f + H}{z_{*f}} \tag{7}$$

Integrating equation (7) with respect to time yields

$$t = \frac{(\theta_s - \theta_i)}{K_e \cos \gamma} \left[z_{*f} - \frac{(s_f + H)}{\cos \gamma} \ln \frac{z_{*f} \cos \gamma + s_f + H}{s_f + H} \right] \tag{8}$$

Substituting equation (6) into equation (8) yields the simplified form as follows

$$K_e t \cos \gamma = I - \frac{SM}{\cos \gamma} \ln \left[1 + \frac{I \cos \gamma}{SM} \right], \tag{9}$$

where $S = s_f + H$, $M = \theta_s - \theta_i$.

[10] Equation (9) is the key equation in the GA model. It implicitly describes the variation of cumulative infiltration depth with time. Expanding the second term of the right-hand side of equation (9) with a Taylor series on I around point $I = 0$ and keeping the first two terms in the series yields

$$K_e t \approx \frac{1}{2} \frac{I_h^2 \cos^2 \gamma}{SM} \tag{10}$$

where $I_h = I/\cos \gamma$ is the cumulative depth in the vertical direction. According to the converging range of the Taylor series, this solution is only valid for small time. The variable I_h compares infiltration on a sloping surface to that on a horizontal plane, but with the same horizontal projection lengths. Thus

$$\frac{I_h(\gamma)}{I_h(0)} = \frac{1}{\cos \gamma} \tag{11}$$

This indicates that the sloping surface increases the infiltration at small t by a factor of $1/\cos \gamma$, which is the same result as equation (50) of *Philip* [1991], noting the coordinate change. For $t \to \infty$, or for large infiltration depths, equation (9) can be approximated as

$$K_e t \approx I_h \tag{12}$$

which indicates the slope effect decreases with time and vanishes at very large t.

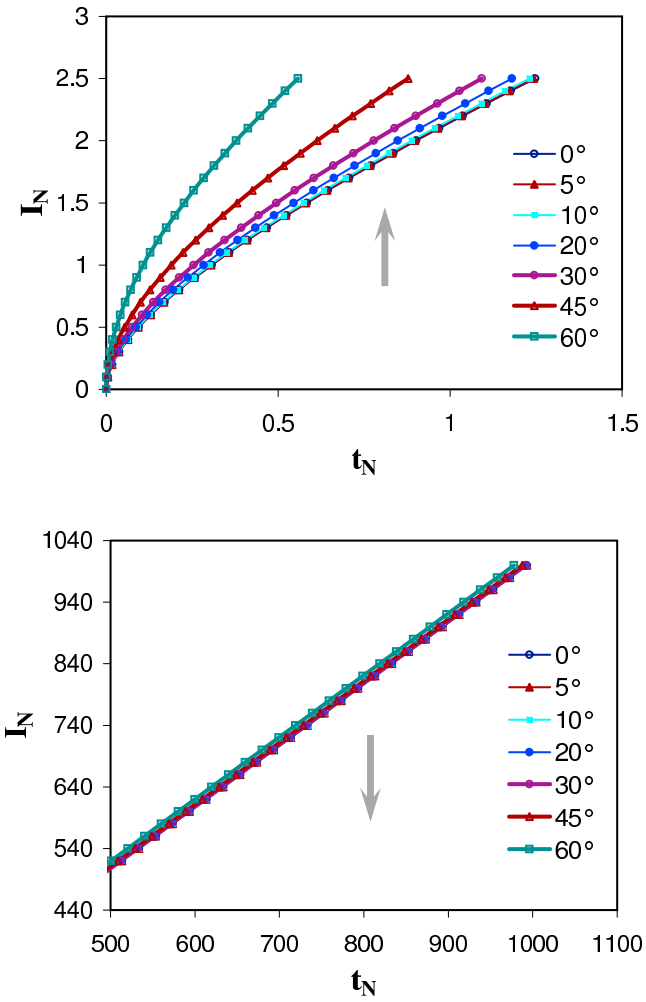

Figure 3. Cumulative infiltration depth versus slope angle and time during ponded infiltration (the arrow shows the sequence of curves with increasing slopes).

[11] Physically, infiltration at small times is controlled by capillary forces, which would be independent of slope angle for homogeneous and isotropic soil. However, increasing the slope angle increases the slope length, and thus increases the total infiltration volume. For large t (or large I), the controlling mechanism becomes gravitationally dominant, which would be reduced by the factor $\cos \gamma$. This effect cancels with increasing slope length, and the slope effect vanishes.

[12] To illustrate, the following nondimensional variables are introduced in

$$t_N = t/t_c; \qquad I_N = \frac{1}{\cos \gamma} \frac{I}{SM} \qquad t_c = \frac{SM}{K_e} \tag{13}$$

where t_N and I_N are dimensionless time and infiltration depth in the vertical direction. The subscript, N, represents the nondimensional variables, t_c is a characteristic time, and $t_c = \dfrac{SM}{K_e}$. Equation (9) can be nondimensionalized as

$$t_N = I_N - \frac{1}{\cos^2 \gamma} \ln \left[1 + I_N \cos^2 \gamma \right] \tag{14}$$

Table 1. Characteristic Time Calculations

Soil Texture	Effective Porosity M	Wetting Front Soil Suction Head S, cm	Hydraulic Conductivity K_e, cm h^{-1}	Characteristic Time t_c, hours
Sand	0.417	4.95	11.78	0.18
Loamy sand	0.401	6.13	2.99	0.82
Sandy loam	0.412	11.01	1.09	4.16
Loam	0.434	8.89	0.34	11.35
Silt loam	0.486	16.68	0.65	12.47
Sandy clay loam	0.330	21.85	0.15	48.07
Clay loam	0.309	20.88	0.10	64.52
Silty clay loam	0.432	27.30	0.10	117.94
Sandy clay	0.321	23.90	0.06	127.87
Silty clay	0.423	29.22	0.05	247.20
Clay	0.385	31.63	0.03	405.92

Figure 3 shows the dimensionless cumulative infiltration depth for different slope angles during ponded infiltration. The differences in infiltration depths between different slope angles are significant for $\gamma > 10°$. For angles less than 10°, the slope effect diminishes. Moreover, for $t_N \gg 1$, the relative differences between different slopes tend to diminish though the absolute differences keep increasing (e.g., at $t_N = 1$, $I_N(30°)/I_N(0°) = 1.16$, with $I_N(30°) - I_N(0°) = 0.32$, while at $t_N = 50$, $I_N(30°)/I_N(0°) = 1.02$ with $I_N(30°) - I_N(0°) = 1$).

[13] It is helpful to give an estimation of the characteristic time t_c. Table 1 is a calculation of t_c for different soil textures. The first three columns are mean values from *Rawls et al.* [1983]. The calculation shows that t_c is on the order of several hours to several days for most soils, except those with very coarse textures. Therefore $t_N \gg 1$ usually corresponds to large time in real-world cases, indicating that small time infiltration is more important in practice.

3.2. Steady Rainfall

[14] For the steady rainfall case, the infiltration rate is calculated using the GA model after ponding (the infiltration rate before ponding is determined by the rainfall intensity). Before and after ponding, GA model can be revised by changing equation (9) into the following form

$$\begin{aligned} i &= p\cos\gamma && t \le t_p \\ K_e\left[t - \left(t_p - t_s\right)\right]\cos\gamma &= I - \frac{SM}{\cos\gamma}\ln\left[1 + \frac{I\cos\gamma}{SM}\right] && t > t_p \end{aligned} \tag{15}$$

where p is the rainfall intensity, assuming raindrops fall in a vertical direction (Figure 1), t_p is the time of ponding, $t - (t_p - t_s)$ is an equivalent time to ponded infiltration, and t_s is a virtual time that represents the time before total infiltration depth reaches I_p, the total infiltration depth in the normal direction when ponding occurs, assuming the infiltration process starts from a ponding status. Thus equation (5) is converted into

$$i = K_e\left(\cos\gamma + \frac{SM}{I}\right) \tag{16}$$

and use equations (15) and (16) to calculate t_s, I_p and t_p as

$$K_e t_s\cos\gamma = I_p - \frac{SM}{\cos\gamma}\ln\left[1 + \frac{I_p\cos\gamma}{SM}\right] \tag{17}$$

$$I_p = \frac{SM}{p\cos\gamma/K_e - \cos\gamma} \qquad (\text{where } i = p\cos\gamma), \tag{18}$$

$$t_p = I_p/p\cos\gamma = \frac{SM}{\frac{p^2\cos^2\gamma}{K_e} - p\cos^2\gamma} \tag{19}$$

We can then compare infiltration on a sloping surface with slope angle γ versus that expected on a horizontal plane under the same steady rainfall event using equations (18) and (19):

$$I_{hp}(\gamma) = I_{hp}(0)/\cos^2\gamma \tag{20}$$

$$t_p(\gamma) = t_p(0)/\cos^2\gamma \tag{21}$$

where I_{hp} is the vertical infiltration depth when ponding occurs.

[15] Equations (20) and (21) indicate that on a surface with slope angle γ, the cumulative infiltration depth needed for occurrence of ponding is larger than that on a horizontal plane, and the ponding time is delayed by the slope angle. The results imply that runoff can be reduced on a sloping surface.

[16] As done above, equations (15) through (19) are normalized as follows

$$t_N - t_{N,p} + t_{N,s} = I_N - \tfrac{1}{\cos^2\gamma}\ln[1 + I_N\cos^2\gamma] \tag{22}$$

$$t_{N,s} = I_{N,p} - \frac{1}{\cos^2\gamma}\ln\left[1 + I_{N,p}\cos^2\right] \tag{23}$$

$$I_{N,p} = \frac{1}{p_N\cos^2\gamma - \cos^2\gamma} \tag{24}$$

$$t_{N,p} = \frac{1}{p_N^2\cos^2\gamma - \cos^2\gamma} \tag{25}$$

where p_N is the dimensionless rainfall intensity, $p_N = p/K_e$.

[17] Figure 4 shows nondimensional infiltration for different slope angles under different rainfall intensities, where increases in infiltration are seen with increases in slope angle. It is also found that rainfall intensity has a significant impact on the infiltration process. For the high rainfall intensity case, cumulative infiltration is similar to the ponded infiltration case because t_p and I_{hp} are small. However, at low rainfall intensity, the infiltration curves diverge after a relatively long time before ponding occurs on any slope. At any given time, the cumulative infiltration depth, I_{hp}, increases with slope angle as well as rainfall intensity.

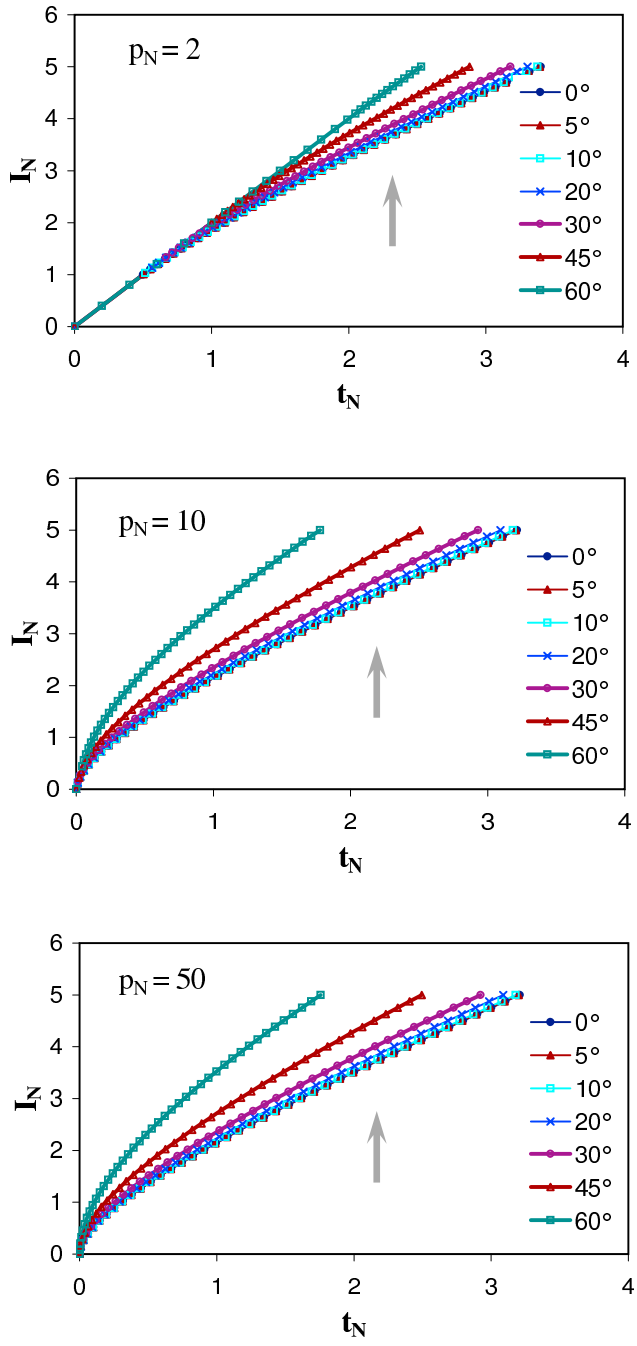

Figure 4. Infiltration process under constant rainfall intensity (the arrow shows the sequence of curves with increasing slopes).

[18] Figure 5 illustrates the total rainfall excess R_N (i.e., the portion of rainfall that potentially becomes runoff). The ponding time increases with increasing slope angle while it decreases with increasing rainfall intensity. The difference in rainfall excesses on different slope angles can be more significant at low rainfall intensity because most of the rainfall infiltrates. However, the results still show that the slope impact is small for slope angles $\gamma < 10°$.

3.3. For Unsteady Rainfall

[19] The infiltration process for conditions of unsteady rainfall on sloping surfaces has basically the same trends as those seen with steady rainfall cases. For the sake of convenience, the detailed derivation is presented in the appendix.

4. Discussion

4.1. Green-Ampt Versus Richards' Equation

[20] To examine our model performance, the results of the proposed GA model were compared to Richards' equation for cases of infiltration through a horizontal

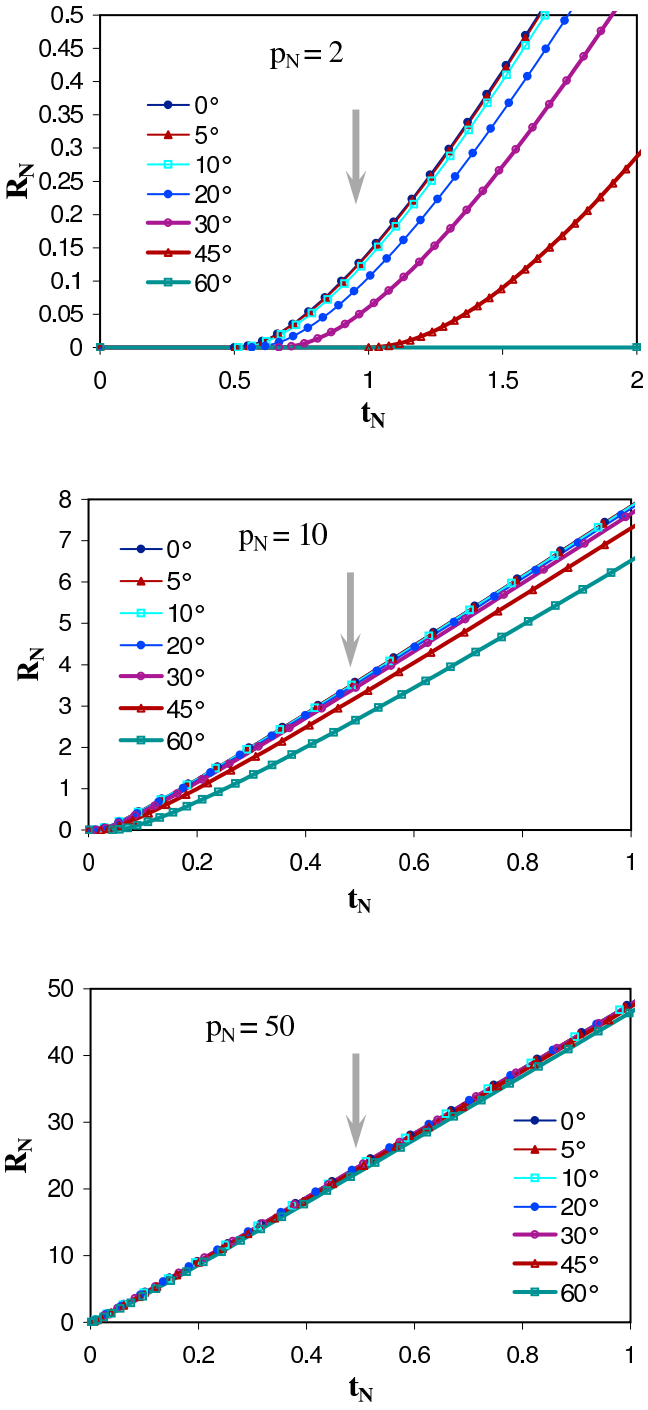

Figure 5. Rainfall excess under constant rainfall intensity (the arrow shows the sequence of curves with increasing slopes).

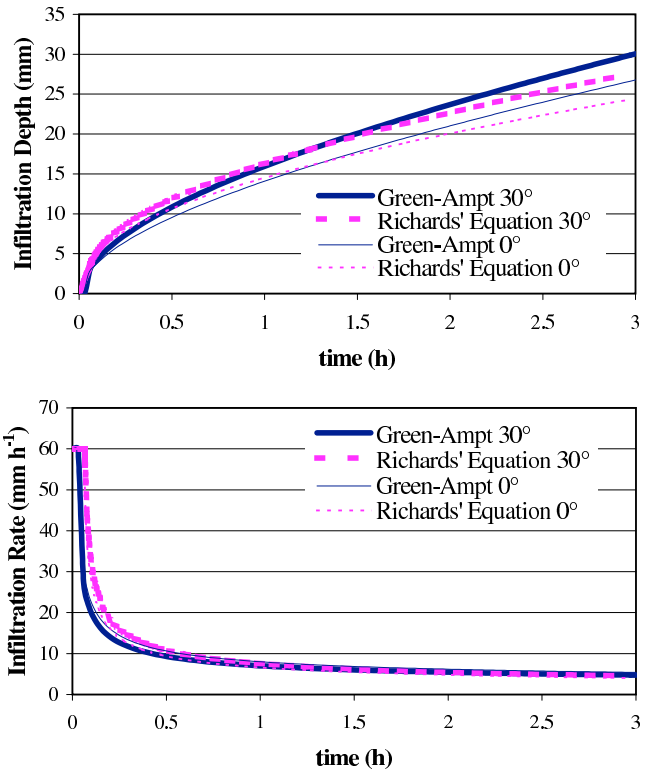

Figure 6. Comparison of GA model and Richards' equation for horizontal plane and a 30° sloping surface under a rainfall of 60 mm h^{-1} intensity.

surface and a surface at 30° for a given soil and rainfall event. The soil water parameters applied in this simulation follow the conventions of *van Genuchten* [1980] for saturated water content (θ_s = 0.46 m^3 m^{-3}), residual water content (θ_r = 0.034 m^3 m^{-3}), empirical parameters n = 1.37 and α = 0.0016 mm^{-1}, and K_s = 2.5 mm hr^{-1}. The initial water content (θ_i) was uniformly set at 0.15 m^3 m^{-3}. The wetting front matric potential for the GA model was calculated using

$$s_f = \frac{1}{K_s - K_i}\int_{\psi_i}^{0} K(\psi)d\psi \tag{26}$$

[*Neuman*, 1976; *Smith*, 2002] where ψ is capillary head (m), and K_i is hydraulic conductivity at θ_i. Equation (25) gives the result of 100 mm. The hydraulic conductivity was calculated with the van Genuchten-Mualem formula [*Smith*, 2002]. A 3-hour constant rainfall event with an intensity of 60 mm h^{-1} was used in this simulation. Richards' equation is solved using the Hydrus models (i.e., the one-dimensional version [*Simunek et al.*, 1999] for the horizontal plane case and the two-dimensional version [*Simunek et al.*, 2005] for the sloping surface case). The simulation results are shown in Figure 6.

[21] The simulation shows that the original GA model (for the horizontal plane) predicts slightly different results compared to Richards' equation. Here the GA model predicts smaller ponding time, smaller vertical infiltration depth in early time and higher infiltration depth in later time, and higher infiltration rates for most of the time. For the sloping surface case, the proposed model performs well by capturing the trend that the sloping surface enhances infiltration and still closely matching the simulation results of Richards' equation.

4.2. Effect of Nonuniform Slope on Lateral Flow

[22] The model's applicability for nonuniform slope, as it affects lateral flux, was examined by analyzing the order of each term in the mass conservation equation. According to Darcy's law, the flow velocities in the downslope and normal directions are

$$u = \mu K\sin\gamma - \mu K\frac{\partial\psi}{\partial x_*}, \quad v = K\cos\gamma - K\frac{\partial\psi}{\partial z_*} \tag{27}$$

where μ represents soil anisotropy in the downslope direction. The mass conservation equation then reads

$$\frac{\partial\theta}{\partial t} = -\frac{\partial u}{\partial x_*} - \frac{\partial v}{\partial z_*} \tag{28}$$

We denote the characteristic lengths of the flow domain in the x_* and z_* directions as L and Z, respectively, where L is on the order of landscape scale and Z is the wetting front depth. For practical rainfall-infiltration cases, L is usually no less than 10^1 to 10^2 m, and Z is usually on the order of 10^{-2} to 10^0 m at the rainfall event timescale. Therefore Z is often much less than L. If u is on the same order of v or smaller, or $O(u) \le O(v)$, then $\frac{\partial u}{\partial x_*} \ll \frac{\partial v}{\partial z_*}$, or $O(\frac{\partial u}{\partial x_*}) < O(\frac{\partial v}{\partial z_*})$, where O represents the order of magnitude of the variable. This result shows that lateral flow has a small impact on water mass balance in soil or infiltration rate at the landscape scale and can be neglected.

[23] The order of magnitude of u and v are compared by looking at the gravity and capillary terms, respectively. Rewriting equation (27) as $u = u_g + u_c$ and $v = v_g + v_c$ yields

$$\frac{u_g}{v_g} = \frac{\mu K\sin\gamma}{K\cos\gamma} = \mu\tan\gamma, \quad \frac{u_c}{v_c} = \frac{-\mu K\frac{\partial\psi}{\partial x_*}}{-K\frac{\partial\psi}{\partial z_*}} \sim \mu Z/L \tag{29}$$

If the soil is isotropic (μ = 1), then the necessary condition for $O(u) > O(v)$ requires that either $\tan\gamma \gg 1$ or $Z \ge L$. The steepness of the slope does not affect the lateral flux gradient or $\frac{\partial u}{\partial x_*}$ significantly unless γ changes with x_* significantly. Even when $\tan\gamma \gg 1$ and γ changes drastically, the effect is confined to the local scale. Cases for $Z \ge L$ occur only for small-scale (local) topographic elements such as small mounds and depression areas, which do not necessarily cause significant lateral flux. Therefore our model is generally applicable for isotropic soil if topographic heterogeneities at the local scale are not a concern. To obtain better results, nonuniform slopes can be segmented and the model can be applied to each segment. Note also that mild anisotropy does not change the analysis significantly. However, for highly anisotropic soil (i.e., $\mu \gg 1$) the lateral flux gradient may become significant at the larger scale for nonuniform topography and the model must be used with caution.

4.3. Effect of Nonvertical Rainfall

[24] In practice, the rainfall direction may not always be vertical. The gauge-measured rainfall intensity, how-

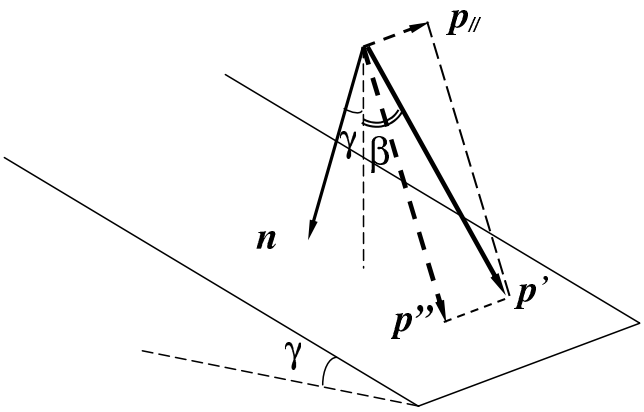

Figure 7. Illustration for nonvertical rainfall.

ever, is actually the rainfall flux normal to a horizontal plane. This uncertainty does affect the rainfall amount received on a sloping surface as well as the infiltration process.

[25] As shown in Figure 7, the situation is considered where the rainfall direction is deflected at an angle β from the vertical direction, and the flux in the actual direction is p'. Therefore the gauge-measured rainfall intensity is $p = p' \cos \beta$. Noting that the angle β and angle γ may be in different planes, the angle between $\boldsymbol{p}'$ and $\boldsymbol{n}$ is denoted as B, so that $\gamma - |\beta| \leq B \leq \gamma + |\beta|$. The angle β is negative if $\boldsymbol{p}'$ deflects upslope. The rainfall flux normal to the slope is $p' \cos B = p \cdot c \cdot \cos \gamma$, where $c = \cos B/(\cos \gamma \cdot \cos \beta)$. To account for this effect, p is simply substituted with pc in equations (15), (18), and (19).

[26] As shown in Figure 8, an arbitrary $\boldsymbol{p}'$ can always be decomposed as $\boldsymbol{p}' = \boldsymbol{p}'' + \boldsymbol{p}_{\|}$, where the $\boldsymbol{p}_{\|}$ is parallel to the slope and $\boldsymbol{p}''$ is in the same vertical plane with $\boldsymbol{n}$. Since $\boldsymbol{p}_{\|}$ has no impact on the infiltration process, only $\boldsymbol{p}''$ is taken into account, or only the case $\boldsymbol{p}' = \boldsymbol{p}''$ is considered, i.e., $B = \beta + \gamma$. Figure 8 shows the modeling results for infiltration for nonvertical rainfall using the proposed GA model. The simulation calculates infiltration for $0° \leq \gamma \leq 45°$ and $-30° \leq \beta \leq 30°$ with a steady vertical rainfall intensity of $p_N = 5$. The total infiltration depth and total runoff at the end time of $t_N = 1$ are plotted. The results show that the deflection angle of rainfall has a relatively small impact on the infiltration process. It does not change the trend of infiltration except for large downslope deflection angles acting on very steep slopes, which decreases the infiltration depth with the slope angle. Upslope deflection increases the infiltration to a small degree and vice versa. As the slope angle decreases, the effect of nonvertical rainfall on infiltration also diminishes. However, the deflection angle does have a large impact on runoff. Even on 5° slopes, the deflection angle can change the runoff by as much as 20 percent, changing the basic relationship of runoff with the slope angle. These differences are mainly caused by the actual rainfall amount received on the slope corresponding to different deflection angles. These results also imply a possible explanation for the conflicting observations reported in previous studies [see *Poesen*, 1984; *Govers*, 1991; *De Ploey et al.*, 1976; *Djorovic*, 1980; *Sharma et al.*, 1983, 1986; *Fox et al.*, 1997; *Chaplot and Le Bissonnais*, 2000]. In those cases, the angle of rainfall relative to the ground surface was not taken into account.

5. Conclusion

[27] The GA model has been physically extended to sloping surfaces. The ponded infiltration and rainfall infiltration processes on sloping surfaces are evaluated using the generalized GA equation. The results address a long-term controversial question of how slope angle affects runoff generation.

[28] Theoretical analyses and numerical computations show that, for vertical rainfall, infiltration increases with the steeper slope angle at small time or low rainfall depths, and the differences tend to vanish at very large time or large rainfall depths. For slope angles less than 10°, the differences are usually small and hence could be neglected without affecting the predictions.

[29] The model was compared to a solution of Richards' equation on a sloping surface and was shown to compare well. The model applicability for nonuniform slope was also discussed through the analysis of significance of lateral flux gradient. The analysis shows the model is generally applicable for isotropic and mild anisotropic soil, if local-scale effects are not important.

[30] The effect of nonvertical rainfall was examined using the modified GA model, and the results show that rainfall angle does not significantly change the infiltration depth, but that it can substantially change the runoff volume to a large extent. The upslope deflection for nonvertical rainfall can reverse the trend of runoff from decreasing to increasing with steeper slopes, which is mainly attributed to the different rainfall amount actually received on the slope.

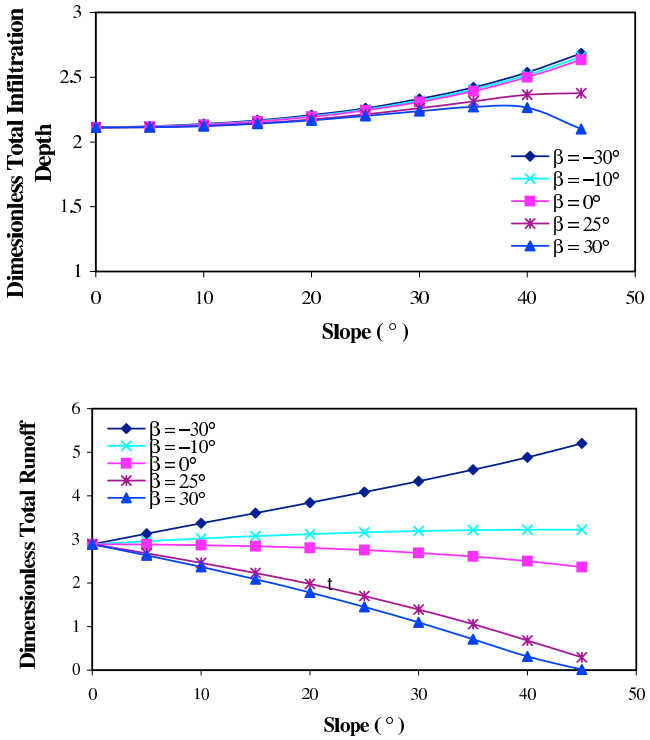

Figure 8. Nonvertical rainfall effect.

[31] The model provides an approach to account for the slope effect for infiltration-runoff process on sloping landscapes. It is applicable to common topography if the distributed modeling approach is employed. This model can be used in hillslope hydrology studies or watershed modeling, where predictions can closely match those of Richards' equation but with less computational cost.

Appendix A: Equations for Unsteady Rainfall Application

[32] For unsteady rainfall events, the main difficulty in solving the infiltration problem is the ponding status and ponding time calculation. Following *Chu* [1978], two indicators are used to determine the ponding status at the end of a time interval. The first indicator, c_u, is used for conditions when ponding has not occurred at time t_{n-1}, the beginning of an interval and the second indicator, c_p, is used for conditions where ponding exists at t_{n-1}. These indicators are defined as follows:

$$c_u = P(t_n)\cos\gamma - R(t_{n-1})\cos\gamma - K_e SM/[p(t_n) - K_e]/\cos\gamma \tag{A1}$$

$$c_p = P(t_n)\cos\gamma - R(t_{n-1})\cos\gamma - I_c(t_n) \tag{A2}$$

where P is the total rainfall depth, R is the total rainfall excess depth in the vertical direction, and I_c is the computed virtual cumulative infiltration depth assuming surface ponding lasts from time t_{n-1} to t_n. The ponding status on the surface at time t_n can be predicted with these two indicators. If $c_u > 0$, ponding occurs before t_n. If $c_u < 0$, no ponding occurs until t_n. If $c_p > 0$, ponding continues t_n. If $c_p < 0$, ponding vanishes before t_n. These conclusions can be derived as follows for four ponding cases, respectively.

A1. Case A

[33] Case A is no ponding at time t_{n-1}, while ponding occurred between t_{n-1} and t_n. The following equation holds in this case:

$$p(t_n)\cos\gamma > i(t_n) = K_s[\cos\gamma + SM]/I(t_n) \tag{A3}$$

therefore

$$I(t_n) > K_e SM/[p(t_n) - K_e]\cos\gamma \tag{A4}$$

because $R(t_{n-1}) < R(t_n)$, and at any time equation $P\cos\gamma - I - R\cos\gamma = 0$ holds, then

$$\begin{aligned} c_u &= P(t_n)\cos\gamma - R(t_{n-1})\cos\gamma - K_e SM/[p(t_n) - K_e]/\cos\gamma \\ &> P(t_n)\cos\gamma - R(t_n)\cos\gamma - I(t_n) = 0 \end{aligned} \tag{A5}$$

A2. Case B

[34] Case B is no ponding at time t_{n-1}, and still no ponding at time t_n. This case requires

$$p(t_n)\cos\gamma < i(t_n) \tag{A6}$$

and

$$I(t_n) < K_e SM/[p(t_n) - K_e]\cos\gamma \tag{A7}$$

because $R(t_{n-1}) = R(t_n)$, same as (A5), the relation becomes

$$c_u < P(t_n)\cos\gamma - R(t_n)\cos\gamma - I(t_n) = 0 \tag{A8}$$

A3. Case C

[35] In case C, ponding exists at time t_{n-1} and ponding continues at t_n. In this case, $p(t_n)\cos\gamma > i(t_n)$, and equation (15) is still valid, i.e., $I_c(t_n) = I(t_n)$, with $R(t_{n-1}) < R(t_n)$, the indicator requires

$$\begin{aligned} c_p &= P(t_n)\cos\gamma - R(t_{n-1})\cos\gamma - I_c(t_n) \\ &> P(t_n)\cos\gamma - R(t_n)\cos\gamma - I(t_n) = 0 \end{aligned} \tag{A9}$$

A4. Case D

[36] In case D, ponding exists at time t_{n-1} but vanishes at t_n. For this situation, the rainfall intensity is less than the infiltration rate, i.e., $p(t_n) < i(t_n)$.The total infiltration depth obtained from equation (15) is larger than the actual value, i.e., $I_c\ (t_n) > I(t_n)$. If this time period is short, the approximate relationship $R(t_{n-1}) = R(t_n)$ holds, therefore

$$c_p < P(t_n)\cos\gamma - R(t_n)\cos\gamma - I(t_n) = 0 \tag{A10}$$

[37] **Acknowledgments.** Funding for this research was provided by the U.S. Army Corp of Engineers under contract DACW42-03-2-0000, Meg Jonas, Program Manager, and by the NSF EPSCoR project EPS 044 7416.

References

Chaplot, V., and Y. Le Bissonnais (2000), Field measurements of interrill erosion under different slopes and plot sizes, *Earth Surf. Processes Landforms*, *24*, 145–153.

Chu, S. T. (1978), Infiltration during unsteady rain, *Water Resour. Res.*, *14*(3), 461–466.

De Ploey, J., J. Savat, and J. Moeyersons (1976), The differential impact of some soil loss factors on flow, runoff creep and rainwash, *Earth Surf. Processes Landforms*, *1*, 151–161.

Djorovic, M. (1980), Slope effect on runoff and erosion, in *Assessment of Erosion*, edited by M. De Boodt and D. Gabriels, pp. 215–225, John Wiley, Hoboken, N. J.

Fox, D. M., R. B. Bryan, and A. G. Price (1997), The influence of slope angle on final infiltration rate for interrill conditions, *Geoderma*, *80*, 181–194.

Govers, G. (1991), A field study on topographical and topsoil effects on runoff generation, *Catena*, *18*, 91–111.

Green, W. H., and G. A. Ampt (1911), Studies on soil physics, *J. Agric. Sci.*, *4*(1), 1–24.

Grosh, J. L., and A. R. Jarrett (1994), Interrill erosion and runoff on very steep slopes, *Trans. ASAE*, *37*(4), 1127–1133.

Kirkby, M. J. (Ed.) (1978), *Hillslope Hydrology*, John Wiley, Hoboken, N. J.

Lal, R. (1976), Soil erosion of Alfisols in western Nigeria: Effects of slope, crop rotation and residue management, *Geoderma*, *16*, 363–375.

Mah, M. G. C., L. A. Douglas, and A. J. Ringrose-voase (1992), Effects of crust development and surface slope on erosion by rainfall, *Soil Sci.*, *154*, 37–43.

Mein, R. G., and C. L. Larson (1973), Modeling infiltration during a steady rain, *Water Resour. Res.*, *9*(2), 384–394.

Neuman, S. P. (1976), Wetting front pressure head in the infiltration model of Green and Ampt, *Water Resour. Res.*, *12*(3), 564–566.

Philip, J. R. (1991), Hillslope infiltration: Planar slopes, *Water Resour. Res.*, *27*(1), 109–117.

Poesen, J. (1984), The influence of slope angle on infiltration rate and Hortonian overland flow volume, *Z. Geomorphol.*, *49*, 117–131.

Rawls, W. J., D. L. Brakensiek, and N. Miller (1983), Green-Ampt infiltration parameters from soils data, *J. Hydraul. Eng.*, *109*(1), 62–70.

Sharma, K., H. Singh, and O. Pareek (1983), Rain water infiltration into a bar loamy sand, *Hydrol. Sci. J.*, *28*, 417–424.

Sharma, K., O. Pareek, and H. Singh (1986), Microcatchment water harvesting for raising Jujube orchards in an arid climate, *Trans. ASEA*, *29*(1), 112–118.

Simunek, J., M. Sejna, and M. T. van Genuchten (1999), The HYDRUS-2D software package for simulating two-dimensional movement of water, heat, and multiple solutes in variably saturated media, version 2.0, *Rep. IGWMC-TPS-53*, Int. Ground Water Model. Cent., Colo. Sch. of Mines, Golden.

Simunek, J., M. T. van Genuchten, and M. Sejna (2005), The HYDRUS-1D software package for simulating the movement of water, heat, and multiple solutes in variably saturated media, version 3.0, *HYDRUS Software Ser. 1*, Dep. of Environ. Sci., Univ. of Calif., Riverside.

Smith, R. E. (2002), *Infiltration Theory for Hydrologic Applications*, *Water Resour. Monogr. Ser.*, vol. 15, AGU, Washington, D. C.

Torres, R., W. E. Dietrich, D. R. Montgomery, S. P. Anderson, and K. Loague (1998), Unsaturated zone processes and hydrologic response of a steep, unchanneled catchment, *Water Resour. Res.*, *34*(8), 1865–1879.

U.S. Army Corps of Engineers (1998), HEC-1 flood hydrograph package, user's manual, version 4.1, Davis, Calif.

van Genuchten, M. T. (1980), A closed-form equation for predicting the hydraulic conductivity of unsaturated soils, *Soil Sci. Soc. Am. J.*, *44*, 892–898.

Wischmeier, W. H., and D. D. Smith (1978), *Predicting Rainfall Erosion Losses*, *Agric. Handb. Ser.*, vol. 537, Agric. Res. Serv., U.S. Dep. of Agric., Washington, D. C.

L. Chen and M. H. Young, Division of Hydrologic Sciences, Desert Research Institute, 755 East Flamingo Road, Las Vegas, NV 89119, USA. (li.chen@dri.edu)